Ferromagnetic instability for the single-band Hubbard model in the strong-coupling regime

Yusuke Kamogawa,[1] Joji Nasu,[1,2] and Akihisa Koga[1]
[1]*Department of Physics, Tokyo Institute of Technology, Meguro, Tokyo 152-8551, Japan*
[2]*Department of Physics, Yokohama National University, 79-5 Tokiwadai, Hodogaya, Yokohama 240-8501, Japan*

(Received 2 April 2019; published 3 June 2019)

We study a ferromagnetic instability in a doped single-band Hubbard model by means of dynamical mean-field theory with the continuous-time quantum Monte Carlo simulations. Examining the effect of the strong correlations in the system on the hypercubic and Bethe lattice, we find that the ferromagnetically ordered state appears in the former, while it does not in the latter. We also reveal that the ferromagnetic order is more stable in the case that the noninteracting density of states (DOS) exhibits a slower decay in the high-energy region. The present results suggest that, in the strong-coupling regime, the high-energy part of DOS plays an essential role for the emergence of the ferromagnetically ordered state, in contrast to the Stoner criterion justified in the weak-interaction limit.

DOI: 10.1103/PhysRevB.99.235107

I. INTRODUCTION

The ferromagnetic (FM) metallic state in the strongly correlated electron systems is a long-standing problem though iron is known to be a magnet from ancient times. In the multiorbital system, there exists the Hund coupling between electrons in degenerate orbitals, which tends to realize the FM ordered states at low temperatures [1–4]. In fact, the ordered state has been reported in the doped Hubbard model with degenerate orbitals [5], and double exchange model [6], which should be relevant for realistic materials such as $La_{1-x}Sr_xMnO_3$ [7]. By contrast, the FM instability in simpler models is less understood. When the Hartree approximation is applied to the single-band Hubbard model, one meets the Stoner criterion, namely, the FM instability appears due to the Coulomb interaction when the system has a large density of states (DOS) at the Fermi level. This criterion is qualitatively correct in the weak-coupling region. In fact, the existence of the FM ordered states has been clarified in the single-band systems with flat bands [8–15] and asymmetric DOS [16–19].

In the case with strong Coulomb interactions, the Stoner theory is not applicable because of the large modulation of the low-temperature susceptibility. To take into account the spin fluctuations, theoretical attempts have been devoted previously [20–22]. In the strong-coupling limit, intersite correlations via the effective Heisenberg interactions should be dominant, which enhances antiferromagnetic (AFM) fluctuations against the FM instability. In the bipartite system in the $d > 1$ dimensions, the AFM ordered state is always realized at half filling [23]. Away from half filling, doped holes should gain kinetic energy, and therefore it is not trivial that the AFM ordered state survives in the strong-coupling limit. On the other hand, Nagaoka has proved that for a single hole in the Hubbard model on a lattice with closed loops the ground state is a fully polarized ferromagnet in this limit, the so-called Nagaoka ferromagnetism [24]. Therefore, it is still controversial how stable such a polarized ordered state is in the system with finite hole density. An important point is that, in this strong-coupling region, large Coulomb interactions and low-energy metallic properties must be taken into account precisely on an equal footing.

In our paper, to discuss the instability of the ferromagnetism we use dynamical mean-field theory (DMFT) [25–28], which is exact in the infinite dimensions and one of the appropriate frameworks to take into account the wide range of energy scales. It has already been clarified that the asymmetry of the DOS plays an important role for realizing the FM state in the weak-coupling region [17–19]. As for the strong-coupling region, it has been clarified that the FM ordered state is not realized in the system on the Bethe lattice [19,29], but in the hypercubic lattice [30,31]. These facts in the strong-coupling region may be understood in terms of the Nagaoka mechanism since there are no closed loops in the Bethe lattice. However, in the framework of DMFT, the lattice structure is involved only via the noninteracting DOS, which should lead to a minor change in the system, e.g., the critical interactions for Mott transitions [32,33]. Therefore, key factors for stabilizing the strong-coupling FM ordered state remain unclear. Furthermore, quantitative treatments are still lacking even in the infinite dimensional systems since with conventional impurity solvers such as the noncrossing approximation [30,34–36] and numerical renormalization group [29,31,32,37–39] it is hard to obtain the dynamical quantities in both low-energy and extremely high-energy regions precisely. To overcome this, in this paper, we make use of the continuous-time quantum Monte Carlo (CTQMC) method [40,41] based on the segment algorithm. We then discuss the FM instability in the system more precisely to determine the finite temperature phase diagram.

The paper is organized as follows. In Sec. II, we introduce the single-band Hubbard model and briefly explain the framework of DMFT. In Sec. III, we consider the infinite dimensional Hubbard model on the hypercubic and Bethe lattices to discuss the FM instability at low temperatures. The effect of the noninteracting DOS is also addressed, by examining magnetic properties in the system with Student-t distribution DOS. A summary is given in the final section.

 ©2019 American Physical Society

II. MODEL AND METHODS

We consider the single-band Hubbard model, which is described by the following Hamiltonian as

$$H = -t \sum_{\langle i,j,\rangle,\sigma} (c^{\dagger}_{i\sigma} c_{j\sigma} + \text{H.c.}) + U \sum_{i} n_{i\uparrow} n_{i\downarrow} - \sum_{i\sigma} \left(\mu + \frac{h}{2}\sigma\right) n_{i\sigma}, \quad (1)$$

where $c_{i\sigma}(c^{\dagger}_{i\sigma})$ annihilates (creates) an electron with spin $\sigma(=\uparrow,\downarrow)$ at the ith site and $n_{i\sigma} = c^{\dagger}_{i\sigma} c_{i\sigma}$. t is the transfer integral, U is the on-site interaction, μ is the chemical potential, and h is the external magnetic field.

To study magnetic properties in the single-band Hubbard model, we make use of DMFT [25–28]. In DMFT, the lattice model is mapped to the problem of a single impurity connected dynamically to a "heat bath." The electron Green's function is obtained via the self-consistent solution of this impurity problem. The treatment is exact in the limit of the infinite dimensions since nonlocal electron correlations are irrelevant. The self-energy is reduced to be site-diagonal $\Sigma_\sigma(k, i\omega_n) = \Sigma_\sigma(i\omega_n)$, where $\omega_n[= (2n+1)\pi T]$ is the Matsubara frequency and T is the temperature. The lattice Green's function is given as

$$G_\sigma(k, i\omega_n)^{-1} = G_{0\sigma}(k, i\omega_n)^{-1} - \Sigma_\sigma(i\omega_n), \quad (2)$$

where $G_{0\sigma}(k, i\omega_n)^{-1} = i\omega_n + \mu + \frac{h}{2}\sigma - \epsilon_k$ and ϵ_k is the dispersion relation. The local Green's function is then obtained as

$$G_{loc,\sigma}(i\omega_n) = \int dk G_\sigma(k, i\omega_n) \quad (3)$$

$$= \int dx \frac{\rho_0(x)}{i\omega_n + \mu + \frac{h}{2}\sigma - x - \Sigma_\sigma(i\omega_n)}, \quad (4)$$

where we introduce the noninteracting DOS $\rho_0(x) = \int dk \delta(x - \epsilon_k)$. In the effective impurity model, the Dyson equation is given as

$$\mathcal{G}_\sigma(i\omega_n)^{-1} = G_{imp,\sigma}(i\omega_n)^{-1} + \Sigma_{imp,\sigma}(i\omega_n), \quad (5)$$

where $\mathcal{G}(i\omega_n)$ is the effective bath. Solving the effective impurity model, one can obtain the self-energy and Green function. We iterate the self-consistency conditions $G_\sigma(i\omega_n) = G_{imp,\sigma}(i\omega_n)$ and $\Sigma_\sigma(i\omega_n) = \Sigma_{imp,\sigma}(i\omega_n)$ until the desired numerical accuracy is achieved.

In our calculations, we make use of the hybridization expansion CTQMC simulations [40,41] based on the segment algorithm, which is one of the powerful methods to solve the effective impurity model. In the method, Monte Carlo samplings are efficiently performed by local updates such as insertion (removal) of a segment or empty space between segments (antisegment), or shifts of segment end points. However, the acceptance probabilities are exponentially suppressed with respect to the interaction strength U. Therefore, it is hard to evaluate the Green's function with a reasonable computational cost when $U \gg t$. Here, we also use additional updates, where the configurations for both spins in a certain interval are simultaneously changed. This allows us to perform the CTQMC method in the strong-coupling region efficiently [42]. Furthermore, we use the intermediate representation for the Green's function [43] since $G_{\text{imp}}(\tau)$ is expected to change rapidly around $\tau = 0, \beta$ in the strong-coupling region.

To discuss magnetic properties in the single-band Hubbard model, we calculate the uniform magnetization and magnetic susceptibility, which are defined as

$$m = \frac{1}{2}\sum_i (\langle n_{i\uparrow}\rangle - \langle n_{i\downarrow}\rangle), \quad (6)$$

$$\chi = \lim_{h\to 0} \frac{m}{h}. \quad (7)$$

In our calculations, the magnetic susceptibility is numerically evaluated by the induced magnetization in the system with a fixed chemical potential since the modulation of the electron number is confirmed to be negligible in the presence of h. Here, we focus on the nature of the FM metallic state in the single-band Hubbard model. For this purpose, we neglect the AFM ordered state and phase separation, which should be realized close to half filling $n \sim 1$ [30,31], where $n = \sum_{i\sigma}\langle n_{i\sigma}\rangle/N$. This simplification allows us to exhibit the essence of the FM instability in the strong-coupling region.

In our paper, we consider the Hubbard model on the Bethe and hypercubic lattices to study their magnetic properties. The corresponding noninteracting DOS, which is important in the framework of DMFT [see Eq. (4)], is given as

$$\rho_b(x) = \frac{2}{\pi D}\sqrt{1 - \left(\frac{x}{D}\right)^2}, \quad (8)$$

$$\rho_{hc}(x) = \frac{1}{\sqrt{\pi} D} \exp\left[-\left(\frac{x}{D}\right)^2\right], \quad (9)$$

where D is the characteristic energy scale. It has been clarified that the difference in the shape of DOS simply leads to the quantitative change in the critical interaction of the Mott transition [32,33]. On the other hand, away from commensurate fillings, the shape has been discussed to be crucial for the instability to the FM ordered state in strongly correlated metals [19,29–31]. In particular, as for the above two forms of the DOS, their high-energy parts are obviously different; the DOS of the hypercubic lattice has an exponentially decaying tail, but that of the Bethe lattice is finite only in the limited region, as shown in Fig. 1. In the following, we discuss the role of the shape of the DOS for the FM instability through systematic finite temperature calculations.

III. NUMERICAL RESULTS

We first consider the Hubbard model on the hypercubic lattice [30,31] to clarify the presence of the FM ordered phase when the system is away from half filling ($n < 1$) in the case of large Coulomb interactions. Figure 2 shows the magnetic susceptibility in the single-band Hubbard model at $T/D = 0.05$ and 0.1. It is found that in the noninteracting system ($U = 0$) the susceptibility little depends on the electron density and temperature in this scale ($\chi D \sim 0.3$). When the interaction strength is much larger than the hopping (bandwidth) and temperature, nonmonotonic behavior appears in the susceptibility as a function of the filling n. The peak structure develops with increasing the Coulomb

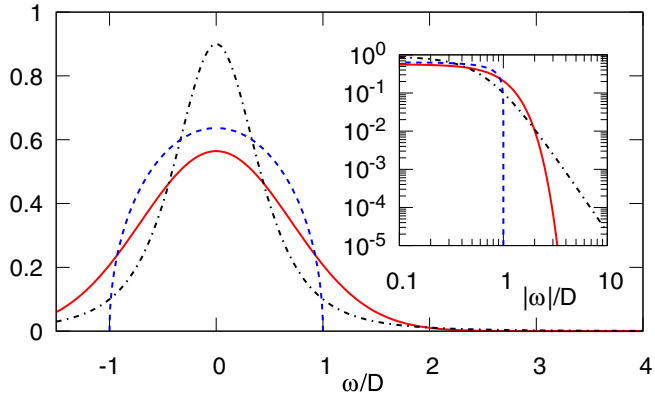

FIG. 1. Solid and dashed lines represent DOS in the noninteracting system on the hypercubic and Bethe lattices. The dot-dashed line represents the Student-t distribution, which will be defined in Eq. (11). The inset shows the tails of their DOS in the large $|\omega|$ region.

interaction and decreasing the temperature. At the low temperature $T/D = 0.05$, the susceptibility has a maximum around $n \sim 0.95$, where ferromagnetic fluctuations are enhanced. This suggests that the FM instability appears away from the half filling when the system has a larger interaction strength at lower temperatures.

To examine the presence of the FM ordered phase at finite interactions and temperatures, we calculate the uniform susceptibility and magnetization in the system with $U/D = 100$ at $T/D = 0.01$, as shown in Fig. 3. In the small n case, the system is in the paramagnetic (PM) state with finite susceptibility. Increasing the electron number, the susceptibility monotonically increases and at last diverges at the critical value $n = n_{c1}$. Beyond the critical value, the finite magnetization is induced, implying that the FM ordered state is realized in the single-band Hubbard model on the hypercubic lattice. The magnetization has a maximum around $n \sim 0.95$ and finally it vanishes at $n = n_{c2}$, where the phase transition occurs again

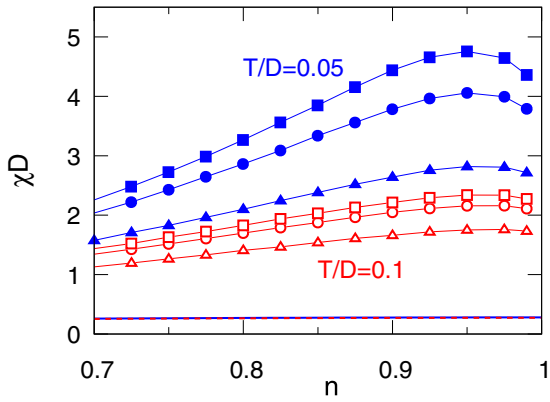

FIG. 2. Magnetic susceptibility as a function of band filling n in the system on the hypercubic lattice when $U/D = 10$ (triangles), 20 (circles), and 30 (squares) at the temperatures $T/D = 0.1$ (open symbols) and 0.05 (solid symbols). Solid and dashed lines around $\chi D \sim 0.3$ are the results for the noninteracting system at $T/D = 0.05$ and 0.1.

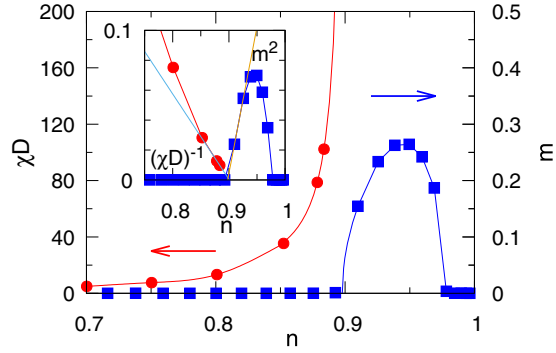

FIG. 3. Uniform magnetic susceptibility and magnetization as a function of the electron density in the system with $U/D = 100$ at the temperature $T/D = 0.01$. The inset shows critical behavior of the susceptibility and magnetization. Solid lines are guides to the eyes.

to the PM metallic state. By examining critical behavior, we obtain the critical densities $n_{c1} = 0.90$ and $n_{c2} = 0.98$.

To reveal how stable the FM ordered state is against thermal fluctuations, we show in Fig. 4 the temperature dependence of the magnetization and magnetic susceptibility in the system with $U/D = 100$ and $n = 0.95$. We find that decreasing temperatures the magnetic susceptibility monotonically increases and at last diverges at a finite temperature T_c. Further decrease of temperatures drives the system to the FM ordered state with the uniform magnetization m. The critical temperature $T_c/D \sim 0.013$ is obtained, examining critical behavior in these quantities $m \sim (T_c - T)^{\beta}$ and $\chi \sim (T - T_c)^{-\gamma}$ with $\beta = 1/2$ and $\gamma = 1$, as shown in the inset of Fig. 4. These critical exponents are consistent with the mean-field theory. On the other hand, in the case with $U/D = 20$, the magnetic susceptibility approaches a finite value with decreasing temperatures, implying that the ground state is the PM metal.

By performing similar calculations for different values of U and n, we obtain the phase diagram at the temperature $T/D = 0.0067$, as shown in Fig. 5(a). It is found

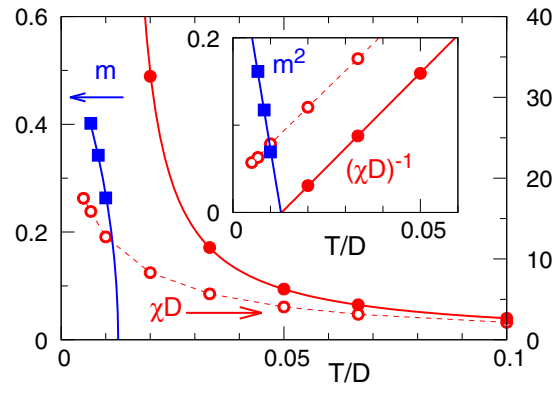

FIG. 4. Solid squares (circles) represent magnetization (magnetic susceptibility) as a function of the temperature in the system on the hypercubic lattice when $U/D = 100$ and $n = 0.95$. Open circles represent the magnetic susceptibility for the system with $U/D = 20.0$ and $n = 0.95$. The inset shows critical behavior of these quantities. Solid and dashes lines are guides to eyes.

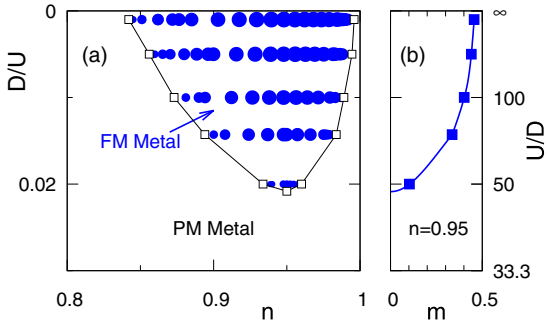

FIG. 5. (a) Phase diagram of the single-band Hubbard model on the hypercubic lattice at the temperature $T/D = 0.0067$. The circle area is proportional to the moment size. (b) Uniform magnetization as a function of the Coulomb interaction in the system with $n = 0.95$ at $T/D = 0.0067$.

that the FM ordered state is realized around $n \sim 0.95$ in the strong-coupling regime. In addition, increasing the interaction strength, the magnetization smoothly increases and approaches a certain value at the fixed temperature, as shown in Fig. 5(b). This means that the FM ordered state becomes stable even in the large U region. This is in contrast to the AFM ordered state at half filling. In the state, the AFM order parameter decreases with increasing the interaction at a fixed temperature since intersite correlations scaled by $\sim t^2/U$ in the strong-coupling limit [42,44]. By contrast, in the case away from the half filing, the uniform magnetization is saturated in the large U limit, as shown in Fig. 5(b). This suggests that the stability of the FM ordered state is dominated by the kinetic energy. This is similar to the origin of the Nagaoka ferromagnetism, implying that the FM ordered state we find is adiabatically connected to the Nagaoka ferromagnetism, which is justified in the limits of $U \to \infty$ and $n \to 1$.

We also examine the ferromagnetism in the Hubbard model on the Bethe lattice with the semielliptical DOS. The results for the magnetic susceptibility at $T/D = 0.05$ and 0.1 are shown in Fig. 6. We find that the susceptibility monotonically increases with increasing n when the temperature and interaction strength are fixed. This suggests that the magnetic instability should appear in the vicinity of the half filling, in contrast to the Hubbard model on the hypercubic lattice discussed above. To examine whether or not the FM ordered state is realized at low temperatures, we also calculate the temperature dependence of the susceptibility for the nearly half-filled system ($n = 0.99$), as shown in Fig. 7. It is found that, in the system with the strong interactions $U/D = 100$ and 200, the magnetic susceptibility monotonically increases with decreasing temperatures. However, we cannot find tendencies toward divergence (see the inset of Fig. 7). This suggests the absence of the FM ordered state in the single-band Hubbard model on the Bethe lattice, which is consistent with the previous works [19,29].

Up to now, we have treated the hypercubic and Bethe lattices to elucidate the origin of the magnetic instability to the FM ordered state in the single-band Hubbard model; the detailed finite temperature calculations clarified that the FM ordered phase appears in the hypercubic lattice, while this does not in the Bethe lattice. These facts might be understood

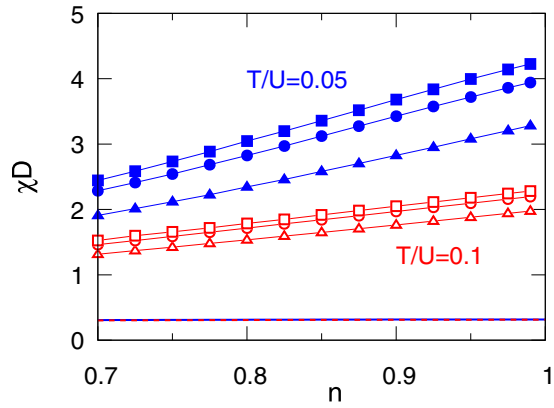

FIG. 6. Magnetic susceptibility as a function of band filling n in the system on the Bethe lattice when $U/D = 10$ (triangles), 20 (circles), and 30 (squares) at the temperatures $T/D = 0.1$ (open symbols) and 0.05 (solid symbols). Solid and dashed lines around $\chi D \sim 0.3$ are the results for the noninteracting system at $T/D = 0.05$ and 0.1.

by the Nagaoka mechanism [24]; in the $U \to \infty$ limit, the FM ordered state is realized in the one-hole doped half-filled system with the closed-loop lattice structure. However, in the framework of DMFT, the lattice structure is indirectly treated only via the noninteracting DOS [Eq. (4)]. Therefore, it may be difficult to conclude that the loop structure plays an essential role in stabilizing the FM ordered state in the infinite dimensions. Now, we focus on the DOS in the noninteracting system. It is clear that the DOSs around the Fermi level are similar to each other. This suggests that the FM ordered state found in the present system with large interactions is not attributed to the DOS at the Fermi energy, which is crucial for the FM ordered state caused by the Slater mechanism justified in the weak-coupling limit.

On the other hand, in the high-energy region, there exists a clear difference in DOS; $\rho_b = 0$ for the Bethe lattice, while $\rho_{hc} \neq 0$ for the hypercubic lattice. This expects that the asymptotic form of DOS away from the Fermi level plays

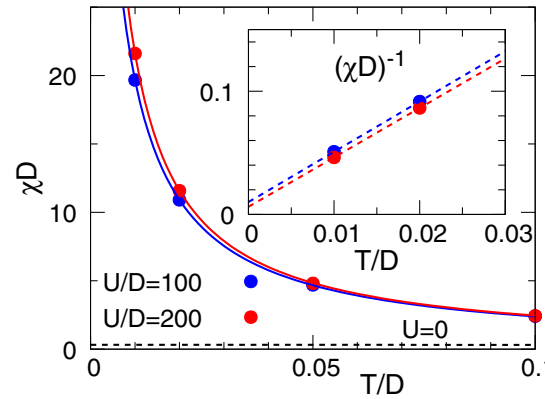

FIG. 7. Magnetic susceptibility as a function of the temperature in the system on the Bethe lattice in the slightly doped systems $n = 0.99$ with $U/D = 100$ and 200. The inset shows the inverse of the susceptibility. Dashed lines are deduced from two data for $T/D = 0.01$ and 0.02.

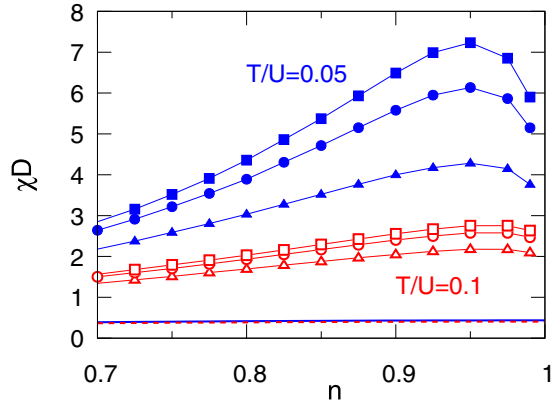

FIG. 8. Magnetic susceptibility as a function of band filling n in the system with Student-t distribution with $\nu = 3$ when $U/D = 10$ (triangles), 20 (circles), and 30 (squares) at the temperatures $T/D = 0.1$ (open symbols) and 0.05 (solid symbols). Solid and dashed lines around $\chi D \sim 0.3$ are the results for the noninteracting system at $T/D = 0.05$ and 0.1.

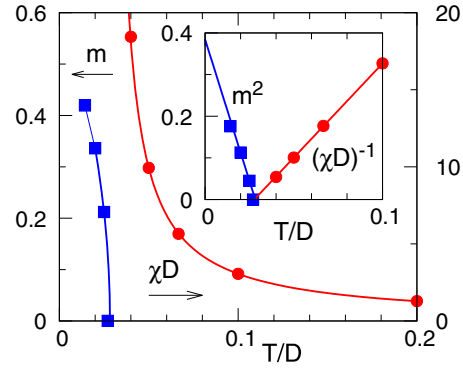

FIG. 9. Magnetization and magnetic susceptibility as a function of the temperature in the system with Student-t distribution when $U/D = 100$ and $n = 0.95$. The inset shows critical behavior of the susceptibility and magnetization. Solid lines are guides to the eyes.

an important role in stabilizing the FM ordered state in the strong-coupling limit. Here, we introduce another function form, the so-called Student-t distribution [45]:

$$\rho_t(x,\nu) = \frac{\Gamma\left(\frac{\nu+1}{2}\right)}{\sqrt{\pi\nu}\Gamma\left(\frac{\nu}{2}\right)}\left[1+\frac{1}{\nu}x^2\right]^{-\frac{\nu+1}{2}}, \tag{10}$$

where $\Gamma(x)$ is the Gamma function. This is reduced to the Cauchy-Lorentz distribution in the case $\nu = 1$ and the Gaussian distribution (hypercubic) in the case $\nu \to \infty$. As an example, we consider the Student-t distribution with $\nu = 3$:

$$\rho_t(x,3) = \frac{1}{\sqrt{2}\pi D}\left[\left(\frac{x}{D}\right)^2+\frac{1}{2}\right]^{-2}, \tag{11}$$

where D is the unit of energy, which is determined such that its variance coincides with that of the DOS of the hypercubic lattice given in Eq. (9). The filling dependence of the magnetic susceptibility in the system with $\rho_t(x,3)$ is shown in Fig. 8. We find that nonmonotonic behavior appears in the magnetic susceptibility and the maximum of the curves is located around $n \sim 0.95$ at $T/D = 0.1$. The results are similar to those for the hypercubic lattice, which expects that the FM ordered state is realized in a finite parameter space unlike the case of the Bethe lattice. Figure 9 shows the magnetization and susceptibility in the system with $U/D = 100$ and $n \sim 0.95$. Decreasing temperatures, the susceptibility diverges at the critical temperature $T_c/D = 0.028$ and the magnetization appears below the temperature. This temperature is larger than that in the case with the Gaussian DOS, indicating that the FM ordered state in the system with the Student-t distribution DOS is more stable than that in the hypercubic system in the case with the strong Coulomb interaction.

IV. SUMMARY

We have studied magnetic properties in the single-band Hubbard model in the infinite dimensions. Combining DMFT with the continuous-time quantum Monte Carlo simulations, we have calculated uniform magnetic susceptibility and magnetization systematically and have found that the FM ordered state is realized in the system on the hypercubic lattice, while no ordered state appears on the Bethe lattice. We have also examined the system with Student-t distribution DOS which has a power-law tail unlike the Gaussian distribution. We have found that the FM ordered state in the system with Student-t distribution is more stable than that in the system on the hypercubic lattice.

The present results suggest that the noninteracting DOS in the high-energy region contributes to the stability of the FM ordered state in the strong-coupling regime while the DOS around the Fermi level is not relevant to the emergence of the FM ordered phase. This is in contrast to the Stoner ferromagnetism in the weak-coupling limit, where the DOS at the Fermi energy is crucial for the emergence of ferromagnetism.

As for finite dimensional systems without the high-energy DOS such as square and cubic lattices, it may be possible to stabilize the FM ordered state due to nonlocal correlations, which could not be taken into account in the framework of DMFT. It is an interesting problem to discuss the FM instability, which is now under consideration.

ACKNOWLEDGMENTS

We would like to thank J. Otsuki, H. Shinaoka, and P. Werner for valuable comments. Parts of the numerical calculations were performed in the supercomputing systems in The Institute for Solid State Physics (ISSP), the University of Tokyo. This work was supported by a Grant-in-Aid for Scientific Research from Japan Society for the Promotion of Science, KAKENHI Grants No. JP18K04678, No. JP17K05536 (A.K.), No. JP16K17747, No. JP16H02206, and No. JP18H04223 (J.N.). The simulations have been performed using some of the ALPS libraries [46].

[1] J. C. Slater, Phys. Rev. **49**, 537 (1936).
[2] J. C. Slater, Phys. Rev. **49**, 931 (1936).
[3] C. Zener, Phys. Rev. **81**, 440 (1951).
[4] J. M. Van Vleck, Rev. Mod. Phys. **25**, 220 (1953).
[5] T. Momoi and K. Kubo, Phys. Rev. B **58**, R567 (1998).
[6] Y. Motome and N. Furukawa, J. Phys. Soc. Jpn. **69**, 3785 (2000).
[7] Y. Tokura, A. Urushibara, Y. Moritomo, T. Arima, A. Asamitsu, G. Kido, and N. Furukawa, J. Phys. Soc. Jpn. **63**, 3931 (1994).
[8] A. Mielke, J. Phys. A **24**, 3311 (1991).
[9] A. Mielke, J. Phys. A **25**, 4335 (1992).
[10] A. Mielke, Phys. Lett. A **174**, 443 (1993).
[11] H. Tasaki, Phys. Rev. Lett. **69**, 1608 (1992).
[12] K. Kusakabe and H. Aoki, Phys. Rev. Lett. **72**, 144 (1994).
[13] S. Miyahara, K. Kubo, H. Ono, Y. Shimomura, and N. Furukawa, J. Phys. Soc. Jpn. **74**, 1918 (2005).
[14] K. Noda, A. Koga, N. Kawakami, and T. Pruschke, Phys. Rev. A **80**, 063622 (2009).
[15] M. Maksymenko, A. Honecker, R. Moessner, J. Richter, and O. Derzhko, Phys. Rev. Lett. **109**, 096404 (2012).
[16] J. Kanamori, Prog. Theor. Phys. **30**, 275 (1963).
[17] M. Ulmke, Eur. Phys. J. B **1**, 301 (1998).
[18] J. Wahle, N. Blümer, J. Schlipf, K. Held, and D. Vollhardt, Phys. Rev. B **58**, 12749 (1998).
[19] M. Balzer and M. Potthoff, Phys. Rev. B **82**, 174441 (2010).
[20] K. K. Murata and S. Doniach, Phys. Rev. Lett. **29**, 285 (1972).
[21] T. Moriya and A. Kawabata, J. Phys. Soc. Jpn. **34**, 639 (1973).
[22] T. Moriya and Y. Takahashi, J. Phys. Soc. Jpn. **45**, 397 (1978).
[23] A. Koga and H. Tsunetsugu, Phys. Rev. B **96**, 214402 (2017).
[24] Y. Nagaoka, Phys. Rev. **147**, 392 (1966).
[25] W. Metzner and D. Vollhardt, Phys. Rev. Lett. **62**, 324 (1989).
[26] E. Müller-Hartmann, Z. Phys. B **74**, 507 (1989).
[27] A. Georges, G. Kotliar, W. Krauth, and M. J. Rozenberg, Rev. Mod. Phys. **68**, 13 (1996).
[28] T. Pruschke, M. Jarrell, and J. Freericks, Adv. Phys. **44**, 187 (1995).
[29] R. Peters and T. Pruschke, New J. Phys. **11**, 083022 (2009).
[30] T. Obermeier, T. Pruschke, and J. Keller, Phys. Rev. B **56**, R8479 (1997).
[31] R. Zitzler, T. Pruschke, and R. Bulla, Eur. Phys. J. B **27**, 473 (2002).
[32] R. Bulla, Phys. Rev. Lett. **83**, 136 (1999).
[33] M. Potthoff, Eur. Phys. J. B **36**, 335 (2003).
[34] N. Grewe and H. Keiter, Phys. Rev. B **24**, 4420 (1981).
[35] Y. Kuramoto, Z. Phys. B **53**, 37 (1983).
[36] M. Eckstein and P. Werner, Phys. Rev. B **82**, 115115 (2010).
[37] H. R. Krishna-murthy, J. W. Wilkins, and K. G. Wilson, Phys. Rev. B **21**, 1003 (1980).
[38] R. Bulla, T. A. Costi, and T. Pruschke, Rev. Mod. Phys. **80**, 395 (2008).
[39] O. Sakai and Y. Kuramoto, Solid State Commun. **89**, 307 (1994).
[40] P. Werner, A. Comanac, L. de' Medici, M. Troyer, and A. J. Millis, Phys. Rev. Lett. **97**, 076405 (2006).
[41] E. Gull, A. J. Millis, A. I. Lichtenstein, A. N. Rubtsov, M. Troyer, and P. Werner, Rev. Mod. Phys. **83**, 349 (2011).
[42] A. Koga and P. Werner, Phys. Rev. A **84**, 023638 (2011).
[43] H. Shinaoka, J. Otsuki, M. Ohzeki, and K. Yoshimi, Phys. Rev. B **96**, 035147 (2017).
[44] H. Yanatori and A. Koga, Phys. Rev. B **94**, 041110(R) (2016).
[45] STUDENT, Biometrika **6**, 1 (1908).
[46] B. Bauer, L. D. Carr, H. G. Evertz, A. Feiguin, J. Freire, S. Fuchs, L. Gamper, J. Gukelberger, E. Gull, S. Guertler, A. Hehn, R. Igarashi, S. V. Isakov, D. Koop, P. N. Ma, P. Mates, H. Matsuo, O. Parcollet, G. P. owski, J. D. Picon, L. Pollet, E. Santos, V. W. Scarola, U. Schollwöck, C. Silva, B. Surer, S. Todo, S. Trebst, M. Troyer, M. L. Wall, P. Werner, and S. Wessel, J. Stat. Mech. (2011) P05001.